nature neuroscience

A single GluN2 subunit residue controls NMDA receptor channel properties via intersubunit interaction

Beth Siegler Retchless[1,2], Wei Gao[1,2] & Jon W Johnson[1]

NMDA receptors (NMDARs) are glutamate-gated ion channels that are present at most excitatory mammalian synapses. The four GluN2 subunits (GluN2A–D) contribute to four diheteromeric NMDAR subtypes that have divergent physiological and pathological roles. Channel properties that are fundamental to NMDAR function vary among subtypes. We investigated the amino acid residues responsible for variations in channel properties by creating and examining NMDARs containing mutant GluN2 subunits. We found that the NMDAR subtype specificity of three crucial channel properties, Mg^{2+} block, selective permeability to Ca^{2+} and single-channel conductance, were all controlled primarily by the residue at a single GluN2 site in the M3 transmembrane region. Mutant cycle analysis guided by molecular modeling revealed that a GluN2-GluN1 subunit interaction mediates the site's effects. We conclude that a single GluN2 subunit residue couples with the pore-forming loop of the GluN1 subunit to create naturally occurring variations in NMDAR properties that are critical to synaptic plasticity and learning.

© 2012 Nature America, Inc. All rights reserved.

Glutamate mediates the majority of fast excitatory neurotransmission in the vertebrate brain. Glutamate receptors (GluRs) transduce signals in two ways: metabotropic GluRs signal via intracellular G proteins and ionotropic GluRs (iGluRs) open intrinsic ion channels in response to agonist binding. NMDARs are glutamate- and glycine-gated iGluRs that are critical for spatial learning, contextual fear memory acquisition and synaptogenesis[1,2]. Particularly high Ca^{2+} permeability and strongly voltage-dependent channel block by external Mg^{2+} distinguish NMDARs from other iGluRs[2]. Mg^{2+} channel block of NMDARs inhibits current influx through the majority of agonist-bound, open NMDARs at resting membrane potentials, but this block is relieved by depolarization. Thus, substantial current flow through NMDARs requires coincident presynaptic activity (glutamate release) and postsynaptic activity (depolarization to relieve Mg^{2+} channel block), conferring on NMDARs a coincidence detection capability that is critical to, for example, NMDAR-dependent long-term potentiation (LTP). LTP strengthens synapses following coincident pre- and postsynaptic activity and is necessary for many types of learning and memory[1]. To mediate this and other important functions, NMDARs require tight regulation of the voltage-dependent Mg^{2+} block that controls current flow and Ca^{2+} influx.

Most NMDARs are tetramers that are thought to be composed of two GluN1 and two GluN2 subunits[2]. Each GluN1 and GluN2 subunit contains an N-terminal domain, an extracellular agonist-binding domain, three transmembrane regions (M1, M3 and M4), a re-entrant loop (M2/p-loop) with a pore-lining segment and an intracellular C-terminal domain[2] (**Fig. 1a**). The p-loop, which forms the narrowest part of the pore toward the intracellular aspect of the channel, creates the selectivity filter[2]. The M1, M3 and M4 regions participate in forming the large extracellular vestibule just external to the selectivity filter[3,4].

Both GluN1 and GluN2 subunits are necessary for the formation of functional glutamate-gated NMDARs in mammalian systems[2]. Expression of the four principal NMDAR subtypes, defined by the GluN2 subunit that is coassembled with GluN1 (GluN1/2A–GluN1/2D receptors), is highly regulated and varies by brain region, developmental stage, experience and disease state[5–7], suggesting that NMDAR subtypes have distinct physiological roles. Triheteromeric receptors composed of GluN1 and two different types of GluN2 subunits also are widely expressed[2], although their functional properties are not well characterized.

The GluN2 subunit present in a receptor shapes numerous NMDAR properties, which therefore vary among NMDAR subtypes. The NMDAR subtype-dependence of several properties, including channel open probability and agonist potency, are largely conferred by the N-terminal domain and the linker to the agonist binding domain[8,9]. Less understood are the structural bases of the NMDAR subtype dependence of open channel properties, including single-channel conductance, Ca^{2+} permeability and Mg^{2+} block. The NMDAR subtype–dependent variation in Mg^{2+} block has been found to depend on three portions of the M1–M4 regions, as well as the agonist-binding domain[10,11]. To the best of our knowledge, there is no information on the origin of the NMDAR subtype dependence of Ca^{2+} permeability or single-channel conductance.

RESULTS

To identify a structural basis for the NMDAR subtype dependence of Mg^{2+} block, we took advantage of clustering of open channel properties that divide NMDARs into two groups: GluN1/2A and GluN1/2B receptors versus GluN1/2C and GluN1/2D receptors. GluN1/2A and GluN1/2B receptors exhibit similarly high Mg^{2+} affinities and single-channel conductances, whereas GluN1/2C and GluN1/2D receptors exhibit similarly low Mg^{2+} affinities and single-channel conductances[6].

[1]Department of Neuroscience and Center for Neuroscience, University of Pittsburgh, Pittsburgh, Pennsylvania, USA. [2]Present addresses: Department of Molecular and Cell Biology, University of California, Berkeley, Berkeley, California, USA (B.S.R.), Kresge Hearing Research Institute, University of Michigan, Ann Arbor, Michigan, USA (W.G.). Correspondence should be addressed to J.W.J. (jjohnson@pitt.edu).

Received 19 October 2011; accepted 13 December 2011; published online 15 January 2012; doi:10.1038/nn.3025

Similarly, GluN1/2A and GluN1/2B receptors have higher Ca^{2+} permeability than GluN1/2C receptors[12,13] (the Ca^{2+} permeability of GluN1/2D receptors has not been quantified). Furthermore, in the M1–M4 regions, GluN2A and GluN2B subunits have more sequence identity with each other than with GluN2C or GluN2D subunits; GluN2C and GluN2D subunits also share more sequence identity with each other than with the other GluN2 subunits (**Fig. 1b**). We targeted sites in the M1–M4 regions for mutagenesis on the basis of this pattern (**Fig. 1b**): sites at which GluN2A and GluN2B subunits contain the same residue, but at which GluN2C and GluN2D subunits share a different residue. In GluN2A subunits, the wild-type residue was substituted with the residue found in GluN2C and GluN2D subunits.

We compared the Mg^{2+} block properties of receptors composed of GluN1 combined with wild-type GluN2A, wild-type GluN2D or mutant GluN2A subunits. For each NMDAR subunit combination, the Mg^{2+} IC_{50} (the [Mg^{2+}] necessary to inhibit 50% of NMDAR-mediated current) was quantified (**Fig. 2a**,**b**). Data were typically gathered at several voltages because of the strong voltage dependence of Mg^{2+} block of NMDARs. Consistent with previous findings[5,10,14,15], GluN1/2A receptors had lower Mg^{2+} IC_{50} values than GluN1/2D receptors across voltages (**Fig. 2b**,**d**).

One residue controls NMDAR subtype dependence of Mg^{2+} block

We measured the Mg^{2+} IC_{50}s of NMDARs with the GluN2C and GluN2D subunit residue substituted at the corresponding GluN2A subunit site. Six mutant GluN1/2A receptors, each containing a single substitution, displayed Mg^{2+} IC_{50}s that were comparable to those of wild-type GluN1/2A receptors (**Figs. 1b** and **2c**,**e**,**f**). NMDARS in which the GluN2C and GluN2D leucine (L) was substituted in place of the GluN2A and GluN2B serine (S) at GluN2A(S632) in M3, however, resulted in Mg^{2+} IC_{50}s that were notably similar to GluN1/2D receptor Mg^{2+} IC_{50}s (**Fig. 2g**).

Investigation of the influence of GluN2A(S632) on the interaction of Mg^{2+} with NMDARs required careful measurement of the voltage dependence of Mg^{2+} IC_{50} from numerous wild-type and mutant receptors (see below). Characterization of the voltage dependence of Mg^{2+} IC_{50} using the protocol described above (**Fig. 2a**) was relatively inefficient. We therefore developed a method to rapidly determine NMDAR Mg^{2+} IC_{50} at seven voltages from −115 mV to −15 mV by measuring *I-V* curves near the end of 5-s applications of each Mg^{2+}-containing solution (**Supplementary Fig. 1a**,**b**). This protocol yielded results similar to those made with the slower protocol (**Fig. 2a** and **Supplementary Fig. 1c–e**). Both protocols revealed that GluN1/2A (S632L) receptor Mg^{2+} IC_{50}s were very close to those of GluN1/2D receptors (**Figs. 2g** and **3a**). Substitution of leucine for serine at this site (the GluN2 S/L site) accounted for 88% of the difference between GluN1/2A and GluN1/2D receptor Mg^{2+} IC_{50}s (averaged across voltages, Online Methods). We then performed the reverse mutation by substituting serine for the homologous leucine at the GluN2 S/L site in GluN2C and GluN2D subunits. The GluN1/2D(L657S) and GluN1/2C(L643S) receptor Mg^{2+} IC_{50}s were decreased toward those of GluN1/2A receptors by an average of 57% and 67%, respectively (**Fig. 3b**,**c**). GluN2 subunit regions that may account for the remaining 33–43% of the NMDAR subtype dependence of Mg^{2+} IC_{50} are considered in the Discussion.

Effect of the GluN2 S/L site on relative Ca^{2+} permeability

To determine whether the effects of the GluN2 S/L site are specific to Mg^{2+} IC_{50}, we examined selective permeability to Ca^{2+}, another NMDAR subtype–dependent channel property of central physiological importance. GluN1/2A and GluN1/2B receptors display similarly high Ca^{2+} permeabilities[13], whereas GluN1/2C receptors display moderately lower Ca^{2+} permeability[12]. To the best of our knowledge, the relative Ca^{2+} permeability of GluN1/2D receptors has not been quantified. We used reversal potential (V_{rev}) measurements to quantify Ca^{2+} permeability relative to Cs^{+} permeability (P_{Ca}/P_{Cs}). V_{rev} values were determined with a voltage-step protocol in bi-ionic conditions in which the sole permeant intracellular ion was Cs^{+} (146 mM) and the sole permeant extracellular ion was either 143 mM Cs^{+} (**Fig. 4a**) or 1.8 mM Ca^{2+} (**Fig. 4b**; Online Methods). We found no significant differences when the V_{rev} values in 143 mM extracellular Cs^{+} of the four wild-type and two mutant NMDARs were compared (one-way ANOVA, $P = 0.45$; **Fig. 4c** and **Supplementary Table 1**). We therefore performed model-independent statistical comparison of Ca^{2+} permeability on the basis of V_{rev} values in 1.8 mM extracellular

© 2012 Nature America, Inc. All rights reserved.

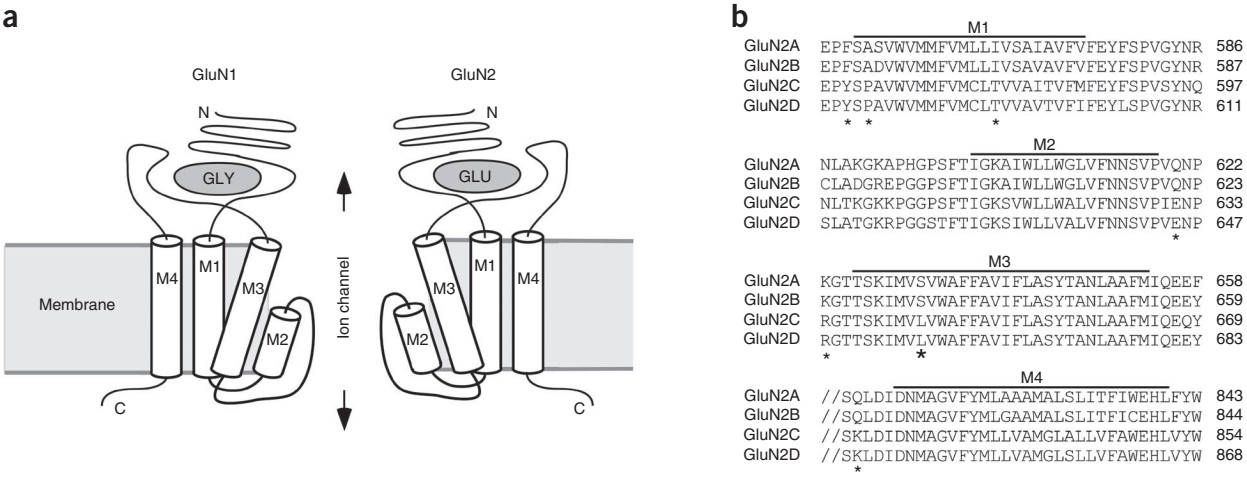

Figure 1 Transmembrane topology and sequence alignment of NMDARs. (**a**) NMDAR transmembrane topology. Each NMDAR subunit contains extracellular N-terminal and agonist-binding domains, three transmembrane regions (M1, M3, M4), a re-entrant loop (M2/p-loop), and an intracellular C-terminal domain. For clarity, only two of the four subunits are shown. This depiction does not indicate subunit arrangement around the pore. (**b**) Amino acid residue sequence alignment of the M1–M4 regions of GluN2A–D subunits, with membrane regions labeled. Slashes indicate sequence discontinuity. Asterisks mark the residues that we studied. The large asterisk marks the GluN2 S/L site.

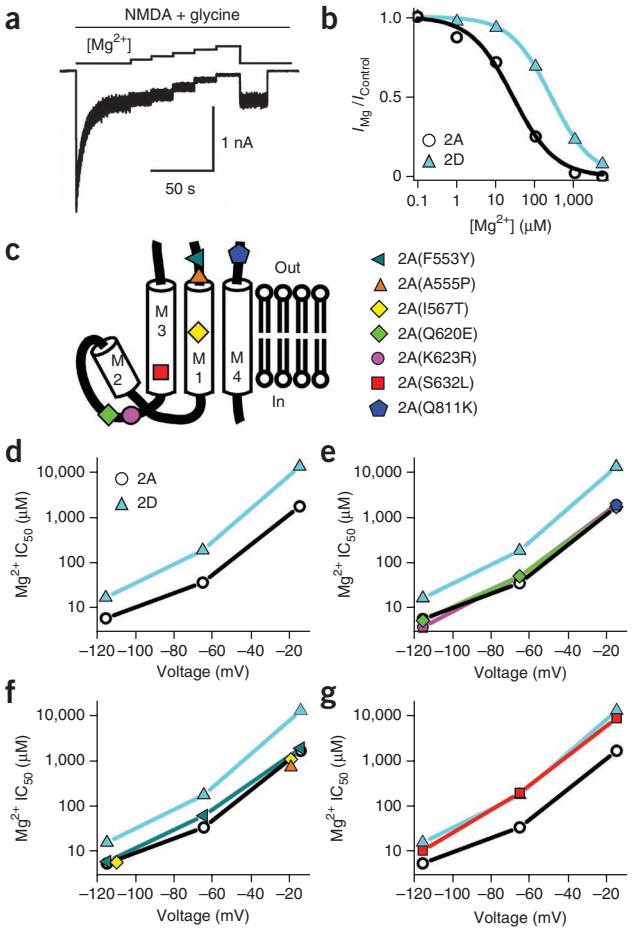

Figure 2 Search for GluN2 residues that affect the NMDAR subtype specificity of Mg^{2+} block. (**a**) Example trace of GluN1/2A receptor–mediated currents at –65 mV and current inhibition by addition of Mg^{2+} at concentrations from 1 μM to 5 mM. (**b**) Mg^{2+}-inhibition curves constructed from the GluN1/2A trace in **a** (black circles) and similar data from GluN1/2D receptors (blue triangles). (**c**) Transmembrane topology of GluN2 subunits and approximate locations of targeted residues. (**d**–**g**) Plots of average Mg^{2+} IC_{50} values at –115, –65 and –15 mV in wild-type receptors and receptors containing amino acid residue substitutions (point mutants in which a residue in the GluN2A subunit was replaced with the homologous residue found in GluN2C and GluN2D subunits). The mutant subunit represented by each symbol is defined in **c** (right). The Mg^{2+} IC_{50}s of wild-type GluN1/2A and GluN1/2D receptors are shown in **d** (these data are replotted in **e**–**g**), the Mg^{2+} IC_{50} values of GluN1/2A(Q620E), GluN1/2A(K623R), GluN1/2A(Q811K) and wild-type receptors are shown in **e**, the Mg^{2+} IC_{50} values of GluN1/2A(F553Y), GluN1/2A(A555P), GluN1/2A(I567T) and wild-type receptors are shown in **f**, and the Mg^{2+} IC_{50} values of GluN1/2A(S632L) and wild-type receptors are shown in **f** (n = 2–24 cells per point).

Ca^{2+} (V_{rev} values of the four wild-type and two mutant NMDARs were compared using one-way ANOVA followed by Tukey *post hoc* comparison). We first will focus on comparisons among wild-type receptors. GluN1/2A and GluN1/2B receptor V_{rev} values were not significantly different (P = 0.99), GluN1/C and GluN1/2D receptor values were not significantly different (P = 0.77), and GluN1/2A and GluN1/2B receptor values were significantly different from GluN1/C and GluN1/2D receptor values (P < 0.03 for each of the four comparisons; **Fig. 4d**). We also calculated P_{Ca}/P_{Cs} ratios by inserting average V_{rev} values into a modified version of the Lewis equation (Online Methods, equation (2))[16,17]. Consistent with previously reported data, GluN1/2A and GluN1/2B receptor P_{Ca}/P_{Cs} ratios were similar and each was higher than the P_{Ca}/P_{Cs} ratio of GluN1/2C receptors (**Fig. 4e**). The GluN1/2D receptor P_{Ca}/P_{Cs} ratio was similar to the P_{Ca}/P_{Cs} ratio of GluN1/2C receptors and lower than the P_{Ca}/P_{Cs} ratios of GluN1/2A and GluN1/2B receptors (**Fig. 4e**). Thus, the subtype-dependent clustering of open-channel properties includes selective permeability to Ca^{2+} as well as Mg^{2+} IC_{50} and single-channel conductance.

When we compared mutant and wild-type NMDARs in 1.8 mM Ca^{2+}, we found that GluN1/2A(S632L) receptor V_{rev} values were significantly different from those of wild-type GluN1/2A receptors (P = 0.018), but not from GluN1/2C (P = 0.99) or GluN1/2D (P = 0.53) receptor V_{rev} values (**Fig. 4d**). GluN1/2D(L657S) receptor V_{rev} values in 1.8 mM Ca^{2+} were significantly different from GluN1/2D receptor V_{rev} values (P = 0.006), but not from GluN1/2A (P = 0.67) or GluN1/2B (P = 0.96) receptor V_{rev} values (**Fig. 4d**). The P_{Ca}/P_{Cs} ratio for GluN1/2A (S632L) receptors was lower than the ratio for GluN1/2A receptors and the P_{Ca}/P_{Cs} ratio for GluN1/2D(L657S) receptors was higher than the ratio for GluN1/2D receptors (**Fig. 4e**). Thus, the GluN2 S/L site regulates the NMDAR subtype dependence of selective permeability to Ca^{2+} as well as Mg^{2+} IC_{50}.

Effects of GluN2 S/L site on single-channel conductance

We also examined the effect of the GluN2 S/L site on the NMDAR subtype dependence of single-channel conductance. Single-channel conductance, along with reversal potential, defines how much current passes through an open channel at any voltage. It is a hallmark characteristic that distinguishes NMDAR subtypes, and determination of single-channel conductance is an important tool for identifying NMDAR subunit composition of native channels in the nervous system[18,19].

We compared single-channel currents (**Fig. 5a**), current amplitudes (**Fig. 5b**) and conductances (**Fig. 5c**) from GluN1/2A, GluN1/2A (S632L), GluN1/2D and GluN1/2D(L657S) receptors. The main state conductance of wild-type GluN1/2A receptors was 54.6 ± 2.1 pS, similar to other reported values[20]. The main state conductance of

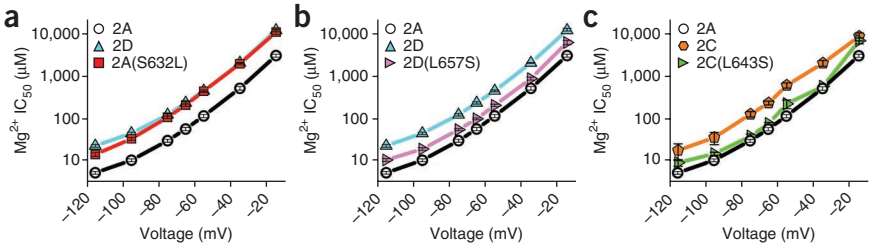

Figure 3 The GluN2 S/L site regulates the NMDAR subtype specificity of Mg^{2+} block. (**a**) GluN1/2A(S632L) receptor Mg^{2+} IC_{50} values were similar to those of the GluN1/2D receptor across a wide range of voltages. The voltage dependence of the Mg^{2+} IC_{50} values of GluN1/2A, GluN1/2D and GluN1/2A(S632L) receptors are plotted. IC_{50} values were determined using a rapid measurement protocol (**Supplementary Fig. 1**). (**b**) GluN1/2D(L657S) receptor Mg^{2+} IC_{50} values approached those of GluN1/2A receptors across a wide range of voltages. (**c**) GluN1/2C(L643S) receptor Mg^{2+} IC_{50} values approached GluN1/2A receptor Mg^{2+} IC_{50}s across a wide range of voltages. Error bars represent s.e.m.

© 2012 Nature America, Inc. All rights reserved.

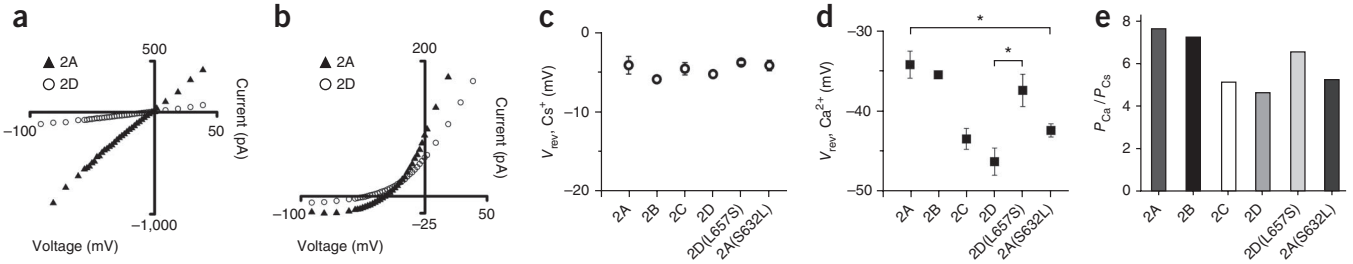

Figure 4 The GluN2 S/L site contributes to NMDAR subtype specificity of relative Ca^{2+} permeability. (**a**,**b**) Representative *I-V* curves in 143 mM extracellular Cs^+ (**a**) and 1.8 mM extracellular Ca^{2+} (**b**). (**c**,**d**) Average V_{rev} ± s.e.m. of wild-type and mutant NMDARs in 143 mM extracellular Cs^+ (**c**) and 1.8 mM extracellular Ca^{2+} (**d**). No significant differences were detected among wild-type and mutant receptor V_{rev} in 143 mM extracellular Cs^+ (one-way ANOVA, $P = 0.45$). Significantly different V_{rev} values (one-way ANOVA followed by Tukey *post hoc* comparison, $P < 0.05$) between wild-type and mutant receptors are marked with an asterisk. (**e**) P_{Ca}/P_{Cs} values of wild-type and mutant NMDARs.

GluN1/2A(S632L) receptors was 34.8 ± 1.4 pS, which was significantly different from the GluN1/2A receptor main state conductance (*t* test for heterogeneity of slopes, $P < 0.0001$), but not significantly different ($P = 0.25$) from that of GluN1/2D receptors (37.4 ± 1.3 pS, measured previously[15] and consistent with other reported values[21]). The GluN1/2D(L657S) receptor main state conductance was 54.9 ± 1.5 pS, which was significantly different from the GluN1/2D receptor main state conductance[15] ($P < 0.0001$), but not significantly different from that of GluN1/2A receptors ($P = 0.23$).

Another single-channel property that distinguishes NMDAR subtypes is the prominent subconductance state of ~20 pS that is exhibited by GluN1/2C and GluN1/2D receptors[15,21]; in contrast, GluN1/2A or GluN1/2B receptors exhibit a larger subconductance state (~40 pS)[20] that is less commonly occupied. GluN1/2A(S632L) receptors exhibited a subconductance state with a conductance (17.0 ± 0.7 pS) that was not significantly different from the subconductance state of GluN1/2D receptors (20.2 ± 1.3 pS, $P = 0.052$; **Fig. 5c**). In contrast, the GluN1/2D(L657S) receptor subconductance state was 49.6 ± 5.6 pS, which was significantly higher than that of GluN1/2D receptors ($P < 0.0001$). We could not consistently resolve a subconductance state in GluN1/2A receptors, although a subconductance state of ~40 pS was occupied infrequently in some patches. Our ability to consistently resolve the subconductance state of GluN1/2D and GluN1/2D(L657S) receptors, but not of GluN1/2A receptors, suggests that subconductance state occupancy by GluN1/2D receptors was not markedly reduced by the mutation. Thus, mutation of the GluN2 S/L site in GluN2D receptors has a powerful effect on the conductance of the subconductance state, but appears to have a weaker effect on subconductance state occupancy.

To determine whether single-channel kinetics are influenced by the GluN2 S/L site, we constructed open period and shut time histograms (**Supplementary Fig. 2** and **Supplementary Table 2**) and statistically compared the values of weighted mean open periods. The weighted mean open periods of GluN1/2A and GluN1/2A(S632L) receptors were not significantly different (one-way ANOVA followed by Tukey *post hoc* comparison, $P = 0.70$), nor were the weighted mean open periods of GluN1/2D and GluN1/2D(L657S) receptors ($P = 0.84$; see **Supplementary Table 2**). Thus, consistent with previous studies showing that NMDAR subtype-dependence of channel gating depends on the N-terminal domain[8,9], the GluN2 S/L site does not appear to have a substantial effect on channel kinetics.

We conclude that the naturally occurring residue replacement in GluN2 subunits that we mimicked by creating GluN2A(S632L), GluN2C(L643S) and GluN2D(L657S) subunits underlies fundamental NMDAR subtype–dependent variations in multiple channel characteristics: Mg^{2+} block, relative Ca^{2+} permeability, and single-channel conductance of both main and subconductance states. However, the way in which the GluN2 S/L site affects pore properties is unclear on the basis of the above data.

Mechanism of GluN2 S/L site influence on Mg^{2+} block

To search for the mechanisms by which the GluN2 S/L site transmits its effects to the pore, we created additional GluN2A subunits with mutations at the GluN2 S/L site and tested whether the Mg^{2+} IC_{50}

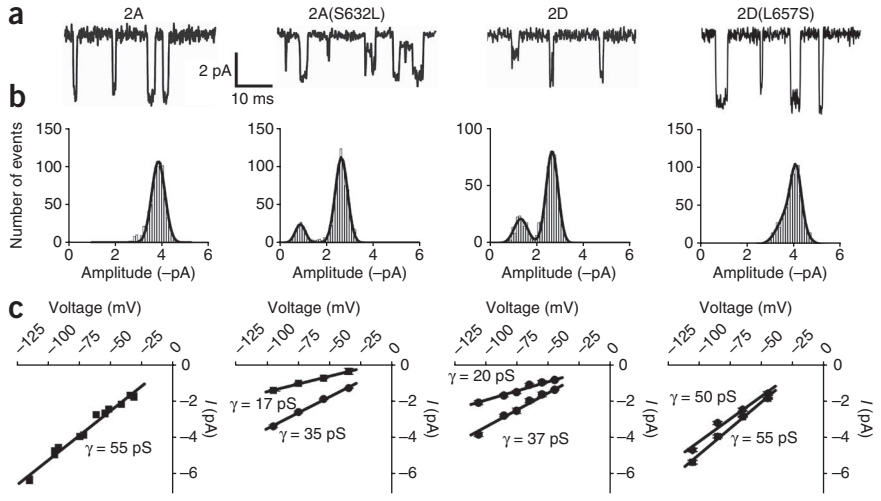

Figure 5 The GluN2 S/L site controls the NMDAR subtype specificity of single-channel conductance. (**a**,**b**) Representative single-channel current traces (**a**) and amplitude histograms (**b**) of GluN1/2A (left), GluN1/2A(S632L) (center left), GluN1/2D (center right) and GluN1/2D(L657S) (right) receptors recorded in the outside-out patch configuration at −75 mV. (**c**) Current versus voltage plots of single-channel currents and linear regression fits. The slope of the linear fit to each plot (single-channel conductance) is shown next to each fit. Left, GluN1/2A receptors ($n = 17$ single-channel current recordings); center left, GluN1/2A(S632L) receptors ($n = 17$); center right, GluN1/2D receptors ($n = 24$; GluN1/2D data from ref. 15); right, GluN1/2D(L657S) receptors ($n = 16$).

© 2012 Nature America, Inc. All rights reserved.

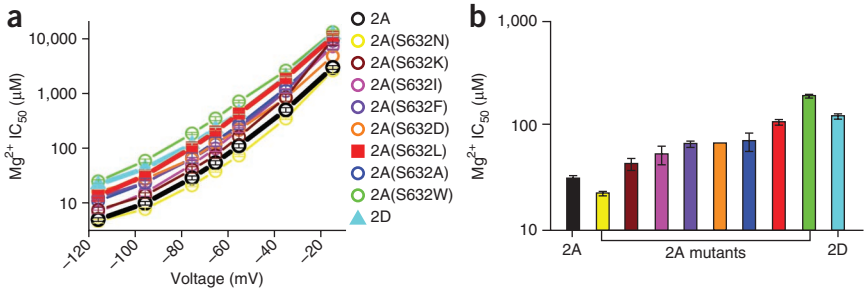

Figure 6 Influence on Mg^{2+} inhibition of mutations at the GluN2 S/L site. (**a**) Voltage dependence of Mg^{2+} IC_{50} of NMDARs containing wild-type GluN2A subunits, wild-type GluN2D subunits or GluN2A subunits mutated at the GluN2 S/L site. (**b**) Mg^{2+} IC_{50} values of wild-type and mutant NMDARs at −75 mV. Examination of correlations between amino acid properties and Mg^{2+} IC_{50}s can be found in **Supplementary Figure 3**. IC_{50} values were determined using a rapid measurement protocol (**Supplementary Fig. 1**). Error bars represent s.e.m.

values of NMDARs containing these mutations correlated with the chemical or physical properties of the substituted amino acid residues. We mutated GluN2A(S632) to asparagine (N), isoleucine (I), lysine (K), phenylalanine (F), aspartate (D), alanine (A) and tryptophan (W), and compared Mg^{2+} IC_{50} values of NMDARs containing GluN2 S/L site point mutant or wild-type subunits (**Fig. 6** and **Supplementary Table 3**). Linear regression analyses to test the dependence of mutant and wild type NMDAR Mg^{2+} IC_{50} values at −75 mV on amino acid polarity, hydrophobicity, hydropathy and volume revealed no substantial correlation (**Supplementary Fig. 3**). We next tried an alternative approach to developing a hypothesis to explain how the GluN2 S/L site regulates channel properties.

The GluN2 S/L site is unlikely to interact with permeant and blocking ions directly because of its location at the base of the M3 region (**Fig. 2c**). We therefore hypothesized that the GluN2 S/L site exerts its influence over Mg^{2+} block, Ca^{2+} permeability and single-channel conductance through interactions with amino acid residues that are closer to the pore. To predict which residues might interact with the GluN2 S/L site, we used the molecular homology modeling software Modeller[22] to create a structural model of the NMDAR M2–M3 region. Homology modeling on the basis of crystallized K^+ channels, particularly the KcsA channel, has been used and validated extensively to predict NMDAR structure and its functional implications[23–25]. The model presented here is based on the crystal structure of the *Bacillus cereus* NaK channel[26]. The NaK channel is a member of the cyclic nucleotide–gated channel family of nonselective tetrameric cation channels, shares high sequence homology with K^+ channels (**Supplementary Fig. 4**), and is probably evolutionarily related to K^+ channels and NMDARs[24,26]. We chose to base the NMDAR homology model on the NaK rather than KcsA channel structure because, similar to NMDARs, the NaK channel is permeable to Na^+ and Ca^{2+} as well as to K^+ (refs. 26,27). We also produced and examined homology models based on the crystal structure of the KcsA channel[28,29] (**Supplementary Fig. 5**). Homology models based on the GluA2 glutamate receptor structure[30] were not initially considered because it was published after we had tested homology model predictions. We subsequently created and examined a homology model based on the GluA2 receptor crystal structure (**Supplementary Discussion** and **Supplementary Fig. 6**).

The NaK channel contains two transmembrane regions (M1 and M2) separated by a re-entrant p-loop. Similar to an upside-down NMDAR channel, the NaK channel p-loop extends from near the extracellular surface of the membrane to approximately halfway through the channel. Several studies have demonstrated the structural conservation of glutamate receptor M2–M3 regions and the homologous regions of proteins related to the NaK channel[23–25,31]; we therefore limited the NaK channel–based homology model to the M2–M3 regions (**Fig. 7a**). To ensure sequence alignment validity, we generated a ClustalX multiple sequence alignment of NMDAR subunits, the NaK channel and nine K^+ channels for which crystal structures of the pore region are available (**Supplementary Fig. 4**). This alignment, which involved no residue insertions or deletions, was consistent with previously published alignments based on both experimental and computational methods[4,23,25,32].

Our GluN1/2A receptor model based on the NaK channel has a GluN1-2A-1-2A subunit arrangement[30] (**Fig. 7b**). The GluN2 S/L site in the model interfaces with the p-loop of GluN1 subunits (**Fig. 7c–e**). When viewed as a space-filling residue, GluN2A(S632) appears to be very close to two GluN1 tryptophans in the p-loop helix, GluN1(W608) and GluN1(W611), which are separated by approximately one α-helical turn (**Fig. 7e**). Our homology model based on the KcsA channel yielded very similar predictions (**Supplementary Fig. 5**). To test experimentally whether GluN1(W608) or GluN1(W611) couples with the GluN2 S/L site to influence GluN2 subunit–dependent channel properties, we performed mutant cycle analyses[33,34]. In a mutant cycle analysis, the effects of two or more point mutations are evaluated to probe for functional evidence of coupling between residues at these sites.

For each mutant cycle, we measured the Mg^{2+} IC_{50} values of four NMDAR subunit combinations: wild-type GluN1 and wild-type GluN2A subunits (wild type/wild type), wild-type GluN1 and mutant GluN2A subunits (wild type/mutant), mutant GluN1 and wild-type GluN2A subunits (mutant/wild type), and mutant GluN1 and mutant GluN2A subunits (mutant/mutant). If there is no coupling between the GluN1 and GluN2 subunit residues, then inclusion of a mutant GluN1 subunit in an NMDAR should result in the same degree of functional change, regardless of whether that mutant GluN1 subunit is expressed with a wild-type or mutant GluN2A subunit. That is, if the mutated residues do not interact, then the magnitude of change in Mg^{2+} IC_{50} from wild type/wild type to mutant/wild type should be equal to the magnitude of change from wild type/mutant to mutant/mutant. Similarly, the magnitude of change in Mg^{2+} IC_{50} from wild type/wild type to wild type/mutant should be the same as that from mutant/wild type to mutant/mutant. Mutant cycle analyses are commonly quantified by calculation of a coupling coefficient, Ω. In our experiments, putative coupling between residues was assessed indirectly by measuring the Mg^{2+} IC_{50} values of each subunit combination.

$$\Omega = \frac{(Mg^{2+}IC_{50}\ \text{wild type/mutant})(Mg^{2+}IC_{50}\ \text{mutant/wild type})}{(Mg^{2+}IC_{50}\ \text{wild type/wild type})(Mg^{2+}IC_{50}\ \text{mutant/mutant})}$$

When Ω = 1, there is no evidence for coupling between two residues. Ω>1 or Ω < 1 argues for coupling between the residues of interest. Ω values do not provide information on the statistical significance of our data. We therefore performed two-way ANOVA interaction tests at each voltage tested (Online Methods) to determine whether the mutant cycles provided statistically significant evidence for residue-residue coupling.

© 2012 Nature America, Inc. All rights reserved.

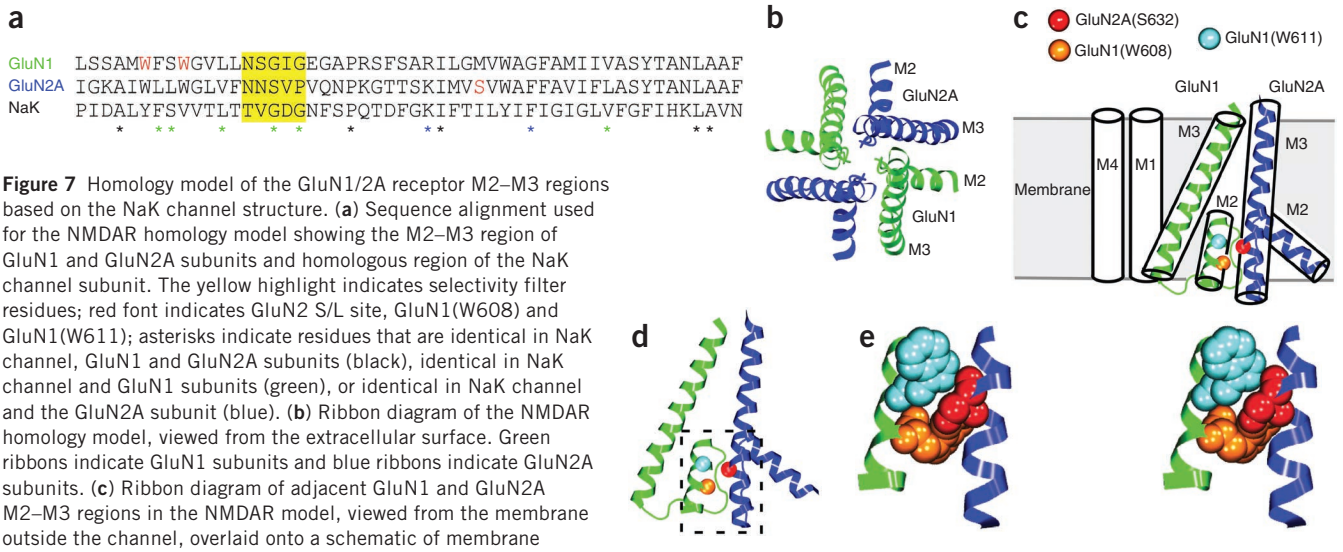

Figure 7 Homology model of the GluN1/2A receptor M2–M3 regions based on the NaK channel structure. (**a**) Sequence alignment used for the NMDAR homology model showing the M2–M3 region of GluN1 and GluN2A subunits and homologous region of the NaK channel subunit. The yellow highlight indicates selectivity filter residues; red font indicates GluN2 S/L site, GluN1(W608) and GluN1(W611); asterisks indicate residues that are identical in NaK channel, GluN1 and GluN2A subunits (black), identical in NaK channel and GluN1 subunits (green), or identical in NaK channel and the GluN2A subunit (blue). (**b**) Ribbon diagram of the NMDAR homology model, viewed from the extracellular surface. Green ribbons indicate GluN1 subunits and blue ribbons indicate GluN2A subunits. (**c**) Ribbon diagram of adjacent GluN1 and GluN2A M2–M3 regions in the NMDAR model, viewed from the membrane outside the channel, overlaid onto a schematic of membrane regions. The α carbons of GluN2A(S632) (red), GluN1(W608) (orange) and GluN1(W611) (cyan) are displayed as spheres. GluN1 and GluN2A subunits on the far side of the channel and schematic of M1 and M4 regions of GluN2A were removed for clarity. (**d**) Ribbon diagram of the NMDAR model, viewed from outside the channel. Spheres indicate α carbons of three residues as in **c**. The GluN1 and GluN2A subunits on the far side of the channel were removed for clarity. (**e**) Stereo view of intersubunit residue-residue interactions in the NMDAR model from the boxed area in **d**. The α-helical sections of GluN1 subunit M2 and GluN2A subunit M3 regions are shown as ribbons. Space-filling residues are colored as in **c**.

We first probed for coupling between GluN1(W611) and GluN2A(S632). Several attempted mutant cycles were unsuccessful because of mutant receptors that expressed currents that were too small to permit accurate measurement of Mg^{2+} IC_{50} (Online Methods). We eventually found that GluN1(W611A) produced currents that were large enough to permit Mg^{2+} IC_{50} measurements when coexpressed with GluN2A and when coexpressed with GluN2A(S632L). Mutating GluN1(W611) to alanine had little effect on Mg^{2+} IC_{50} values when coexpressed with GluN2A, and little effect when coexpressed with GluN2A(S632L) (**Fig. 8a**). Thus, our data do not provide evidence for coupling between GluN1(W611) and GluN2A(S632).

To determine whether GluN1(W608) interacts with the GluN2 S/L site, we replaced GluN1(W608) with serine, creating GluN1(W608S), and replaced the GluN2A serine with tryptophan, creating GluN2A(S632W). We predicted that mutating the GluN1 tryptophan to serine might partially compensate for the effects of mutating the GluN2A serine to tryptophan because the tryptophan and serine would be exchanged in the mutant/mutant receptor. Expression of GluN1(W608S) with wild-type GluN2A slightly increased the Mg^{2+} IC_{50} values compared with GluN1/2A receptor values (**Fig. 8b**). If there is no coupling between GluN1(W608) and GluN2A(S632), then expression of GluN1(W608S) with GluN2A(S632W) similarly should slightly increase the Mg^{2+} IC_{50} values compared with GluN1/2A (S632W) receptor values. Mutating GluN2A(S632) to tryptophan, however, markedly decreased the Mg^{2+} IC_{50} of NMDARs when coexpressed with GluN1(W608S) subunits (**Fig. 8b**). Evidence for coupling was found at every voltage. Thus, mutating GluN1(W608) to serine partially compensates for the effects of mutating GluN2A(S632) to tryptophan. We subsequently performed another mutant cycle

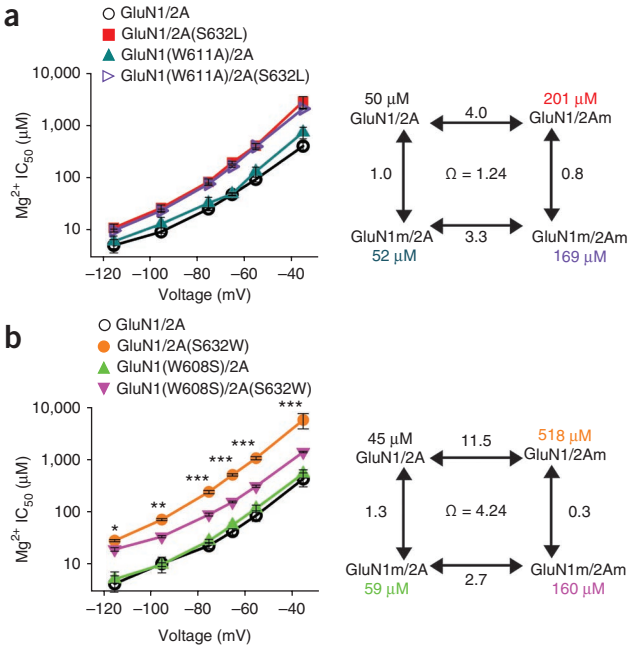

Figure 8 Mutant cycle examination of intersubunit interactions involved in NMDAR subtype specificity of Mg^{2+} block. (**a**,**b**) Mutant cycle results and schematics. Left, plot of the voltage dependence of wild-type and mutant NMDAR Mg^{2+} IC_{50} ($n = 4$ cells for each NMDAR subunit combination). $^{*}P < 0.05$; $^{**}P < 0.01$; $^{***}P < 0.001$. Right, mutant cycle schematic and representative mutant cycle results at –65 mV. GluN1m and 2Am represent mutant subunits. Above each NMDAR subunit combination name is the Mg^{2+} IC_{50}. Adjacent to each arrow is the fold change of Mg^{2+} IC_{50} presented as the ratio (mean Mg^{2+} IC_{50} of NMDARs containing a mutant subunit)/(mean Mg^{2+} IC_{50} of NMDARs containing a wild-type subunit). If a GluN1 residue is not coupled to the GluN2 S/L site, then the fold change of Mg^{2+} IC_{50} should be the same for the left and right vertical arrows and the same for the upper and lower horizontal arrows. The coupling coefficient Ω at –65 mV is in the center of the schematic. The GluN1(W611)-GluN2A(S632) mutant cycle is shown in **a** (two-way ANOVA results: –115 mV, $P = 0.51$; –95 mV, $P = 0.38$; –75 mV, $P = 0.53$; –65 mV, $P = 0.09$; –55 mV, $P = 0.26$; –35 mV, $P = 0.06$. $\Omega = 1.6$, averaged across voltages). The GluN1(W608)-GluN2A(S632) mutant cycle is shown in **b** (two-way ANOVA results: –115 mV, $P = 0.03$; –95 mV, $P = 0.01$; –75 mV, $P = 0.00001$; –65 mV, $P < 0.00001$; –55 mV, $P = 0.00004$; –35 mV, $P = 0.001$. $\Omega = 3.5$, averaged across voltages). IC_{50} values were determined using a rapid measurement protocol (**Supplementary Fig. 1**). Error bars represent s.e.m.

© 2012 Nature America, Inc. All rights reserved.

analysis to test for coupling between GluN1(W608) and GluN2A(S632), but using the mutants GluN1(W608S) and GluN2A(S632L) (**Supplementary Fig. 7**). Evidence for coupling between the residues was still observed, although of smaller magnitude than for the GluN1(W608S) and GluN2A(S632W) cycle. The coupling may be weaker because a tryptophan-serine residue exchange was not performed and/or because mutating GluN2A(S632) to leucine had a smaller effect on Mg^{2+} IC_{50} than mutation to tryptophan.

These mutant cycle data indicate that the NMDAR subtype dependence of Mg^{2+} inhibition depends on coupling between the GluN2 S/L site and GluN1(W608), but leave open the possible involvement of additional pairs of residues. Although residue-residue coupling usually implies close physical proximity of residues[34], it is possible that coupling between residues may result from indirect interactions. Of particular importance, the data unveil an intersubunit interaction between GluN1 and GluN2 that is critical to an NMDAR subtype–dependent channel property.

DISCUSSION

We have identified a naturally occurring residue substitution in GluN2 subunits that is predominantly responsible for the NMDAR subtype dependence of Mg^{2+} inhibition, Ca^{2+} permeability and single-channel conductance. Using structural homology models, we predicted that the GluN2 S/L site, which is at the base of the M3 region, conveys its effects on the pore by interacting with the p-loop of the adjacent GluN1 subunit. The results of mutant cycle experiments support the model's prediction, identifying GluN1(W608) as a p-loop residue that is coupled to the GluN2 S/L site.

On the basis of our results, and those of recent studies, the spectrum of subtype-dependent NMDAR properties can be divided into two clusters. One cluster of properties is related to channel gating and the binding of ligands that influence gating, and includes maximal channel open probability, pH sensitivity, Zn^{2+} inhibition, agonist potency and deactivation kinetics. The NMDAR subtype dependence of this gating property cluster depends principally on the large N-terminal domain and its linker to the agonist binding domain[8,9], which are distant from the GluN2 S/L site. We found that the NMDAR subtype dependence of a second cluster, properties of the open channel, depends, in contrast, on a single amino acid difference in the M3 transmembrane region. Together, differences in and near the N-terminal domain and at the GluN2 S/L site underlie the great majority of functional variation among NMDAR subtypes.

The GluN2 S/L site regulates ion permeation of the NMDAR channel, as demonstrated by its effects on relative Ca^{2+} permeability and single-channel conductance. The influence of the GluN2 S/L site on Mg^{2+} block also may be partly mediated by an effect on ion permeation; the single greatest difference between the kinetics of Mg^{2+} block of GluN1/2A and GluN1/2D receptors is an enhanced rate of Mg^{2+} permeation through GluN1/2D receptors[15,35]. The GluN2 S/L site and GluN1(W608), situated near the intracellular end of the pore, appear to be well located to affect ion permeation.

The subtype dependence of channel block by Mg^{2+} is not solely determined by the GluN2 S/L site. This was particularly clear from measurements showing that GluN2 S/L site leucine to serine mutations accounted for 67% of the Mg^{2+} IC_{50} difference between GluN1/2C and GluN1/2A receptors, and 57% of the difference between GluN1/2D and GluN1/2A receptors (**Fig. 3b**,**c**). Based on previous studies, it appears likely that the remaining NMDAR subtype dependence of Mg^{2+} IC_{50} may be accounted for by multiple subunit regions, including the M1 and M4 transmembrane regions, the M2-M3 linker[10], and the agonist binding domain[11]. Thus, the majority of the NMDAR subtype dependence of Mg^{2+} IC_{50} depends on the single residue difference at the GluN2 S/L site; the remaining NMDAR subtype dependence of Mg^{2+} IC_{50} is likely to depend on a number of the >700 residue differences between GluN2A or GluN2B and GluN2C or GluN2D subunits, spread across several regions of the subunits.

In a series of experiments related to those presented here, Mg^{2+} block of GluN1/2C receptors was examined using GluN2C subunits modified to contain parts of the GluN2B subunit[10]. As noted above, multiple sections of GluN2 subunits were found to influence the NMDAR subtype dependence of Mg^{2+} IC_{50}. It was found that receptors containing a GluN2C subunit with a leucine-to-serine substitution at the GluN2 S/L site exhibited increased voltage dependence of Mg^{2+} block, but no change in Mg^{2+} IC_{50} at −100 mV. The apparent discord between the previous study and our findings may stem from the use of different preparations: *Xenopus* oocytes were used in the previous study[10], whereas we used HEK cells, resulting in multiple experimental differences, including permeant ion concentrations, which strongly affect Mg^{2+} block[36].

Insight into why NMDAR channels exhibit weak monovalent cation selectivity is suggested by comparing selectivity filters of homologous channels with known structures. Although the GluA2 AMPA receptor crystal structure[30] cannot be used because its selectivity filter was not resolved (**Supplementary Discussion**), previous studies have demonstrated structural similarities between NMDARs and K^+ channels[24,37]. The NaK channel is structurally similar to the NMDAR channel, but, unlike K^+ channels, it is cation nonselective[26,27]. In K^+ channels, four K^+ binding sites are formed along the selectivity filter by four rings of carbonyl oxygens projecting into the channel[28,38,39], whereas the NaK channel selectivity filter contains only two rings of carbonyl oxygens[26]. NaK channel residues along the pore-lining section of the p-loop that do not contribute to these carbonyl oxygen rings form an external vestibule that is wider than the selectivity filter; this vestibule appears to contribute to nonspecific cation permeability[27]. The monovalent cation nonselectivity of NMDARs similarly may depend on a relatively short selectivity filter and wide vestibule. The NMDAR selectivity filter nevertheless must exhibit powerful selectivity among divalent cations.

Our mutant cycle results suggest that the GluN2 S/L site regulates the NMDAR subtype specificity of Mg^{2+} block at least in part through coupling with GluN1(W608). The mechanism by which GluN1(W608) mediates communication between the GluN2 S/L site and the pore, however, is unknown. A substituted-cysteine accessibility study showed that GluN1(W608) is solvent accessible from the intracellular, but not the extracellular, aspect of the membrane[40]. Mutations of the homologous residue in GluN2B subunits, also a tryptophan, strongly affect Mg^{2+} block and permeation[41]. Notably, the tryptophan at GluN1(W608) is highly conserved. All known mammalian iGluR subunits contain a tryptophan at homologous positions, with the exception of the GluN3A and GluN3B subunits. In fact, this tryptophan is present at the homologous sites of nematode (*Caenorhabditis elegans*) and insect (*Drosophila melanogaster*) iGluRs, as well as in predicted iGluR subunits and glutamate binding proteins of the plant *Arabidopsis*[42,43]. Furthermore, the tryptophan at this site is conserved in the bacterial GluR0 channel and in some potassium channels[43]. Thus, GluN1(W608) and the tryptophans at equivalent sites in NMDAR subunit homologs are likely to be important for channel function.

METHODS

Methods and any associated references are available in the online version of the paper at http://www.nature.com/natureneuroscience/.

© 2012 Nature America, Inc. All rights reserved.

Note: Supplementary information is available on the Nature Neuroscience website.

ACKNOWLEDGMENTS
The authors thank A. Qian for valuable contributions to and advice on initial experiments, K. Bouch and C. Shiber for excellent technical assistance, M. Pellegrino for generous help with statistical analyses, M. Casio and A. Retchless for helpful discussions and comments on the manuscript, S. Meriney, M. Grabe, D. Wood and members of the Johnson laboratory for helpful discussions, and D. Colquhoun for making available the DC Analysis programs for single-channel analysis. This work was supported by US National Institutes of Health grants R01 MH045817 and associated S1 supplement (J.W.J.) and F31 MH079755 (B.S.R.).

AUTHOR CONTRIBUTIONS
All the authors participated in experimental design and analysis, and in revision of the manuscript. B.S.R. and W.G. performed the experiments. B.S.R. and J.W.J. wrote the manuscript.

COMPETING FINANCIAL INTERESTS
The authors declare no competing financial interests.

Published online at http://www.nature.com/natureneuroscience/.
Reprints and permissions information is available online at http://www.nature.com/reprints/index.html.

© 2012 Nature America, Inc. All rights reserved.

1. Lynch, M.A. Long-term potentiation and memory. *Physiol. Rev.* **84**, 87–136 (2004).
2. Traynelis, S.F. *et al.* Glutamate receptor ion channels: structure, regulation and function. *Pharmacol. Rev.* **62**, 405–496 (2010).
3. Sobolevsky, A.I., Beck, C. & Wollmuth, L.P. Molecular rearrangements of the extracellular vestibule in NMDAR channels during gating. *Neuron* **33**, 75–85 (2002).
4. Beck, C., Wollmuth, L.P., Seeburg, P.H., Sakmann, B. & Kuner, T. NMDAR channel segments forming the extracellular vestibule inferred from the accessibility of substituted cysteines. *Neuron* **22**, 559–570 (1999).
5. Ishii, T. *et al.* Molecular characterization of the family of the *N*-methyl-D-aspartate receptor subunits. *J. Biol. Chem.* **268**, 2836–2843 (1993).
6. Cull-Candy, S.G. & Leszkiewicz, D.N. Role of distinct NMDA receptor subtypes at central synapses. *Sci. STKE* **2004**, re16 (2004).
7. Clinton, S.M. & Meador-Woodruff, J.H. Abnormalities of the NMDA receptor and associated intracellular molecules in the thalamus in schizophrenia and bipolar disorder. *Neuropsychopharmacology* **29**, 1353–1362 (2004).
8. Yuan, H., Hansen, K.B., Vance, K.M., Ogden, K.K. & Traynelis, S.F. Control of NMDA receptor function by the NR2 subunit amino-terminal domain. *J. Neurosci.* **29**, 12045–12058 (2009).
9. Gielen, M., Siegler Retchless, B., Mony, L., Johnson, J.W. & Paoletti, P. Mechanism of differential control of NMDA receptor activity by NR2 subunits. *Nature* **459**, 703–707 (2009).
10. Kuner, T. & Schoepfer, R. Multiple structural elements determine subunit specificity of Mg^{2+} block in NMDA receptor channels. *J. Neurosci.* **16**, 3549–3558 (1996).
11. Wrighton, D.C., Baker, E.J., Chen, P.E. & Wyllie, D.J. Mg2+ and memantine block of rat recombinant NMDA receptors containing chimeric NR2A/2D subunits expressed in *Xenopus laevis* oocytes. *J. Physiol. (Lond.)* **586**, 211–225 (2008).
12. Burnashev, N., Zhou, Z., Neher, E. & Sakmann, B. Fractional calcium currents through recombinant GluR channels of the NMDA, AMPA and kainate receptor subtypes. *J. Physiol. (Lond.)* **485**, 403–418 (1995).
13. Schneggenburger, R. Simultaneous measurement of Ca^{2+} influx and reversal potentials in recombinant N-methyl-D-aspartate receptor channels. *Biophys. J.* **70**, 2165–2174 (1996).
14. Monyer, H. *et al.* Heteromeric NMDA receptors: molecular and functional distinction of subtypes. *Science* **256**, 1217–1221 (1992).
15. Qian, A., Buller, A.L. & Johnson, J.W. NR2 subunit-dependence of NMDA receptor channel block by external Mg^{2+}. *J. Physiol. (Lond.)* **562**, 319–331 (2005).
16. Lewis, C.A. Ion-concentration dependence of the reversal potential and the single channel conductance of ion channels at the frog neuromuscular junction. *J. Physiol. (Lond.)* **286**, 417–445 (1979).
17. Wollmuth, L.P. & Sakmann, B. Different mechanisms of Ca^{2+} transport in NMDA and Ca^{2+}-permeable AMPA glutamate receptor channels. *J. Gen. Physiol.* **112**, 623–636 (1998).
18. Farrant, M., Feldmeyer, D., Takahashi, T. & Cull-Candy, S.G. NMDA receptor channel diversity in the developing cerebellum. *Nature* **368**, 335–339 (1994).
19. Cull-Candy, S.G. *et al.* NMDA receptor diversity in the cerebellum: identification of subunits contributing to functional receptors. *Neuropharmacology* **37**, 1369–1380 (1998).
20. Stern, P., Cik, M., Colquhoun, D. & Stephenson, F.A. Single channel properties of cloned NMDA receptors in a human cell line: comparison with results from *Xenopus* oocytes. *J. Physiol. (Lond.)* **476**, 391–397 (1994).
21. Wyllie, D.J., Behe, P., Nassar, M., Schoepfer, R. & Colquhoun, D. Single-channel currents from recombinant NMDA NR1a/NR2D receptors expressed in *Xenopus* oocytes. *Proc. Biol. Sci.* **263**, 1079–1086 (1996).
22. Eswar, N. *et al.* Comparative protein structure modeling using MODELLER. *Curr. Protoc. Protein Sci.* **2**, 2.9 (2007).
23. Panchenko, V.A., Glasser, C.R. & Mayer, M.L. Structural similarities between glutamate receptor channels and K^+ channels examined by scanning mutagenesis. *J. Gen. Physiol.* **117**, 345–360 (2001).
24. Wood, M.W., VanDongen, H.M. & VanDongen, A.M. Structural conservation of ion conduction pathways in K channels and glutamate receptors. *Proc. Natl. Acad. Sci. USA* **92**, 4882–4886 (1995).
25. Tikhonov, D.B. Ion channels of glutamate receptors: structural modeling. *Mol. Membr. Biol.* **24**, 135–147 (2007).
26. Shi, N., Ye, S., Alam, A., Chen, L. & Jiang, Y. Atomic structure of a Na^+- and K^+-conducting channel. *Nature* **440**, 570–574 (2006).
27. Alam, A., Shi, N. & Jiang, Y. Structural insight into Ca^{2+} specificity in tetrameric cation channels. *Proc. Natl. Acad. Sci. USA* **104**, 15334–15339 (2007).
28. Doyle, D.A. *et al.* The structure of the potassium channel: molecular basis of K^+ conduction and selectivity. *Science* **280**, 69–77 (1998).
29. Cuello, L.G., Jogini, V., Cortes, D.M. & Perozo, E. Structural mechanism of C-type inactivation in K^+ channels. *Nature* **466**, 203–208 (2010).
30. Sobolevsky, A.I., Rosconi, M.P. & Gouaux, E. X-ray structure, symmetry and mechanism of an AMPA-subtype glutamate receptor. *Nature* **462**, 745–756 (2009).
31. Chen, G.Q., Cui, C., Mayer, M.L. & Gouaux, E. Functional characterization of a potassium-selective prokaryotic glutamate receptor. *Nature* **402**, 817–821 (1999).
32. Tikhonov, D.B., Mellor, J.R., Usherwood, P.N. & Magazanik, L.G. Modeling of the pore domain of the GLUR1 channel: homology with K^+ channel and binding of channel blockers. *Biophys. J.* **82**, 1884–1893 (2002).
33. Hidalgo, P. & MacKinnon, R. Revealing the architecture of a K^+ channel pore through mutant cycles with a peptide inhibitor. *Science* **268**, 307–310 (1995).
34. Schreiber, G. & Fersht, A.R. Energetics of protein-protein interactions: analysis of the barnase-barstar interface by single mutations and double mutant cycles. *J. Mol. Biol.* **248**, 478–486 (1995).
35. Qian, A. & Johnson, J.W. Permeant ion effects on external Mg^{2+} block of NR1/2D NMDA receptors. *J. Neurosci.* **26**, 10899–10910 (2006).
36. Antonov, S.M. & Johnson, J.W. Permeant ion regulation of *N*-methyl-D-aspartate receptor channel block by Mg^{2+}. *Proc. Natl. Acad. Sci. USA* **96**, 14571–14576 (1999).
37. Jones, K.S., VanDongen, H.M. & VanDongen, A.M. The NMDA receptor M3 segment is a conserved transduction element coupling ligand binding to channel opening. *J. Neurosci.* **22**, 2044–2053 (2002).
38. Jiang, Y. *et al.* The open pore conformation of potassium channels. *Nature* **417**, 523–526 (2002).
39. Long, S.B., Campbell, E.B. & Mackinnon, R. Crystal structure of a mammalian voltage-dependent Shaker family K^+ channel. *Science* **309**, 897–903 (2005).
40. Kuner, T., Wollmuth, L.P., Karlin, A., Seeburg, P.H. & Sakmann, B. Structure of the NMDA receptor channel M2 segment inferred from the accessibility of substituted cysteines. *Neuron* **17**, 343–352 (1996).
41. Williams, K. *et al.* The selectivity filter of the *N*-methyl-D-aspartate receptor: a tryptophan residue controls block and permeation of Mg^{2+}. *Mol. Pharmacol.* **53**, 933–941 (1998).
42. Chiu, J.C. *et al.* Phylogenetic and expression analysis of the glutamate receptor–like gene family in *Arabidopsis* thaliana. *Mol. Biol. Evol.* **19**, 1066–1082 (2002).
43. Sprengel, R. *et al.* Glutamate receptor channel signatures. *Trends Pharmacol. Sci.* **22**, 7–10 (2001).

ONLINE METHODS

Cell culture and transfection. HEK293T cells (whole-cell experiments; ATCC) and HEK293 cells (single-channel experiments; ATCC) were maintained as previously described[15]. Calcium phosphate transfections[44] or FuGENE transfections (Roche) were performed with a cDNA ratio of 1 eGFP:1 GluN1:2 GluN2 or 1 eGFP:3 GluN1:6 GluN2.

Mutagenesis and cDNA preparation. cDNAs encoding *Rattus* GluN1-1a (GenBank accession number (ACCN) X63255), GluN2A (ACCN M91561), GluN2C (ACCN M91562) and GluN2D (ACCN L31611) subunit genes in ampicillan resistance–encoding plasmids (pcDNA 3.1 or pcDNA1) were mutagenized with the Stratagene Quik-Change XL sited-directed mutagenesis kit. Mutagenized NMDAR subunit cDNAs from isolated colonies were sequenced from 100–200 bases upstream to 100–200 bases downstream of each mutation (University of Pittsburgh Genomics and Proteomics Core Laboratories). In most cases, mutant-containing plasmids from at least two colonies were expressed for electrophysiological experiments to ensure that results did not arise from unintended mutations. Furthermore, the entire coding sequences of the mutant subunits GluN2A(S632L) and GluN2D(L657S) were sequenced (GeneWIZ). The amino acid residue sequence encoded by the GluN2A(S632L) mutant had two differences from the source sequence: the intended mutation (S632L) and S758T. The latter residue (GluN2A(T758)) is present in another GluN2A sequence (ACCN D13211), suggesting that it was present in the wild-type sequence. The amino acid residue sequence encoded by the GluN2D(L657S) mutant had three differences from the source sequence: the intended mutation (L657S), P94R and A305R. The latter two residues (GluN2D(R94) and GluN2D(R305)) are present in another GluN2D sequence (ACCN U08260), suggesting that they were present in the wild-type sequence.

Electrophysiology. Experiments was performed 12–72 h after initiation of transfection. Borosilicate micropipettes of 2–5 MΩ (whole-cell recordings) or 5–11 MΩ (single-channel recordings) resistance were pulled on a Sutter Instruments P-97 electrode puller. Micropipettes used in single-channel recordings were coated with Sylgard 184. In all recordings except for Ca^{2+} permeability experiments (see below), bath solutions were grounded with a silver chloride pellet. The intracellular solution for whole-cell experiments consisted of 125 mM CsCl, 10 mM HEPES and 10 mM EGTA. The intracellular solution composition for single-channel experiments was 115 mM CsFl, 10 mM CsCl, 10 mM HEPES and 10 mM EGTA. CsOH (~30 mM) was added to both intracellular solutions to arrive at pH 7.2 ± 0.05 and 275 ± 5 mOsmol kg^{-1}. The normal extracellular solution, which was used in all experiments except for Ca^{2+} permeability measurements, consisted of 140 mM NaCl, 2.8 mM KCl, 1.0 mM $CaCl_2$ and 10 mM HEPES. The 1.8 mM extracellular Ca^{2+} solution consisted of 140 mM NMDG, 10 mM HEPES and 1.8 mM Ca^{2+} (pH adjusted to 7.2 ± 0.05 with HCl). The 143 mM extracellular Cs^+ solution contained 140 mM CsCl and 10 mM HEPES (pH adjusted to 7.2 ± 0.05 by addition of ~3 mM CsOH). When necessary, sucrose was added to reach 290 ± 10 mOsmol kg^{-1}. NMDAR responses were elicited by 30 μM glycine and 10 μM NMDA (Mg^{2+} IC_{50} experiments), 50 μM glycine and 1 mM glutamate (Ca^{2+} permeability experiments), or 30 μM glycine and 30 μM NMDA (single-channel experiments), referred to as agonists. NMDA was used as an agonist in some experiments to facilitate comparison with previous data[15]. Magnesium-containing solutions were composed of the normal extracellular solution to which agonists and $MgCl_2$ were added.

Outside-out patch and whole-cell currents were amplified using an Axopatch 200B or 200 patch-clamp amplifier (Molecular Devices) and recorded on video tape and/or computer in pClamp version 9 or 10 format (Molecular Devices). Currents were filtered at 1 kHz (whole-cell recordings) or 2.5 kHz (single-channel recordings) with a Warner Instruments LPF-8 and sampled at 20 kHz (whole-cell recordings) or 50 kHz (single-channel recordings). Correction for liquid junction potentials (V_p) between the intracellular and extracellular solutions was applied in all experiments (whole-cell experiments, $V_p = -6.3$ mV in normal extracellular solution, $V_p = -13.0$ mV in 1.8 mM Ca^{2+} extracellular solution; single-channel experiments, $V_p = -9.7$ mV in normal extracellular solution).

We developed a method for rapid measurement of Mg^{2+} IC_{50} at seven voltages (**Supplementary Fig. 1**). Normal (Mg^{2+} free) extracellular solution plus agonists was applied until a steady-state current was reached. Successively higher [Mg^{2+}] (0–10 mM in normal extracellular solution plus agonists) was applied to the cell, using a 5-s application of each [Mg^{2+}], via a gravity-fed ten-barrel fast perfusion system (**Supplementary Fig. 1**). During the last 1.5 s of each solution application, the command voltage was stepped from a holding potential of −65 mV through a series of voltages ranging from −115 mV to −15 mV, in 20-mV increments. Each stepped command voltage was maintained for 210 ms. The current at each command voltage was averaged over the last 150 ms of the voltage step. Before and after application of agonists, baseline current (0 agonists) at each command voltage was measured using the same sequence of voltage steps; baseline currents were averaged and subtracted from the agonist-activated currents in each [Mg^{2+}] at each command voltage to calculate the NMDAR-mediated current. Using this approach, current measurements in ten [Mg^{2+}] values at seven voltages each were made in ~1.5 min. The ten [Mg^{2+}] values covered a wide concentration range so that an accurate estimate of Mg^{2+} IC_{50} could be made at each of the voltages used. A complete dataset for one cell was gathered by repeating this protocol at least three times and averaging the NMDAR-mediated current at each [Mg^{2+}] and command voltage across trials.

For each cell, at each voltage, fractional current ($I_{Mg}/I_{control}$) measured in each [Mg^{2+}] was plotted on a Mg^{2+}-inhibition curve and fit with

$$\frac{I_{Mg}}{I_{Control}} = \frac{1}{1+\left(\frac{[Mg^{2+}]}{IC_{50}}\right)^n} \quad (1)$$

where n is the Hill coefficient, I_{Mg} is the amplitude of agonist-induced current in [Mg^{2+}] and $I_{control}$ is the amplitude of NMDAR-mediated current in 0 Mg^{2+} (**Fig. 2b** and **Supplementary Fig. 1b**).

To assess relative Ca^{2+} permeability (P_{Ca}/P_{Cs}), we measured V_{rev} of mutant and wild-type NMDARs with whole-cell recordings in bi-ionic conditions. Extracellular solution containing a single permeant ion (Cs^+ or Ca^{2+}) was bath-applied via a gravity-fed perfusion system for several minutes to ensure complete solution exchange. Agonists were then bath-applied for 30–60 s, until desensitization was complete. In the continued presence of agonists, the command voltage was stepped from a holding potential of −65 mV (before correction for junction potential) through a series of voltages ranging from −95 mV to −55 mV in 10-mV increments, then stepped from −50 mV to 10 mV in 2-mV increments, and finally from 15 mV to 55 mV in 10-mV increments. Each command voltage was maintained for 210 ms. Subtraction of baseline current was performed as described for Mg^{2+} IC_{50} experiments. We used two approaches to minimize errors resulting from voltage changes at the interface between the bath solution and the AgCl ground pellet that could occur when changing bath solution. First, in some experiments, we grounded the bath through a 3 M KCl agarose bridge to minimize voltage changes at the agarose-bath solution interface and contamination of the bath solution, which was constantly perfused (3–6 ml min^{-1}; bath volume 250–300 μl). Second, in most experiments, we grounded the bath with a gravity-fed flowing KCl bridge. This bridge consisted of a 1-ml syringe filled with 3M KCl into which an AgCl ground pellet was placed, attached to a 32 gauge needle (0.108-mm inner diameter, Hamilton Company). The needle was inserted into the bath efflux tubing, minimizing the possibility of bath solution contamination. Data from experiments in which voltage drift exceeded 2 mV were excluded from analysis. Relative Ca^{2+} permeability was calculated with a modified Lewis equation[16,17]:

$$V_{rev\,(Ca)} - V_{rev\,(Cs)} = \frac{RT}{F}\ln\frac{4\frac{P_{Ca}}{P_{Cs}}\times[Ca^{2+}]_o}{[Cs]_o\times\left(1+e^{\frac{V_{rev\,(Ca)}}{(RT)/F}}\right)} \quad (2)$$

where $[Cs^+]_o$ and $[Ca^{2+}]_o$ are the extracellular concentrations of Cs^+ and Ca^{2+}, and P_{Ca}/P_{Cs} is the permeability ratio of Ca^{2+} to Cs^+.

Single-channel data analysis. Idealization of single-channel currents was performed using the time-course fitting method[45]. To determine single-channel current amplitudes, we fit Gaussian functions to single-channel current amplitude event histograms using the maximum likelihood method[45]. Conductances were calculated as the slope of the best-fit linear regression to an *I-V* graph containing data collected at four or more voltages. Open period and shut time histograms

© 2012 Nature America, Inc. All rights reserved.

doi:10.1038/nn.3025

(**Supplementary Fig. 2** and **Supplementary Table 2**) were constructed from data collected at −75 mV. Only patches in which less than 5% of the openings were double openings were used. Fits consisting of two to four components were generated using the maximum likelihood method. Time course fitting and maximum likelihood fitting were performed using the DC Analysis programs (http://www.ucl.ac.uk/Pharmacology/dcpr95.html) SCAN and EKDIST, respectively.

Structural modeling. The structural homology modeling program Modeller (version 9.7) was used to create energetically plausible models of the NMDAR M2–M3 region, based on homologous regions of the crystalized NaK channel (PBD ID 2AHZ)[26] and KcsA channel (PBD IDs 1BL8 and 3FB5)[28,29], or of the entire NMDAR minus the C terminus and a portion of the p-loop, based on the crystalized GluA2 channel (PDB ID 3KG2). The molecular graphics program VMD[46] was used to visualize NMDAR models and to generate **Figure 7b–e** and **Supplementary Figures 5b–e** and **6**.

Mutant cycle analysis. Several point mutants at each GluN1 and GluN2 subunit site of interest were created. Mutant cycle measurements were performed if whole-cell recordings from HEK293T cells expressing each relevant mutant subunit combination typically yielded NMDAR current amplitudes more negative than −100 pA at −65 mV in 0 Mg^{2+}. Cells with smaller current amplitudes did not yield reliable Mg^{2+}-inhibition curves, especially at less negative voltages. We attempted to perform experiments with GluN1(W611S) and GluN2A(S632W) subunits based on the idea that the tryptophan-serine exchange in the mutant/mutant receptor might partially compensate for the effects of the GluN2A serine to tryptophan mutation. Currents through GluN1(W611S)/2A(S632W) receptors, however, were too small to permit accurate measurement of Mg^{2+} IC_{50}s. We constructed several more GluN1(W611) point mutants, but most appeared to form nonfunctional channels when co-expressed with wild-type or mutant GluN2A subunits. Thus, we performed a mutant cycle using GluN1(W611A) and GluN2A(S632L) subunits (**Fig. 8a**). We attempted to supplement the mutant cycle experiment in which mutant subunits GluN1(W608S) and GluN2A(S632W) were used (**Fig. 8**) with a mutant cycle experiment that paralleled the GluN1(W611A)-GluN2A(S632L) experiments. We observed no NMDAR-mediated current, however, in GluN1(W608A)/2A(S632L) receptors. In each mutant cycle presented, data at −15 mV were excluded because some mutants did not pass enough current to accurately estimate Mg^{2+} IC_{50}s at that voltage.

Statistical analysis. Most statistical tests were performed using Origin 7 (OriginLab). *t* tests for heterogeneity of slopes were performed using the R software environment[47] (http://www.r-project.org/) with Package HH[48]. In **Figures 3**, **6** and **8**, and **Supplementary Figures 3** and **7**, Mg^{2+} IC_{50} data are presented as mean Mg^{2+} IC_{50} value (averaged across cells) ± s.e.m. For each mutant cycle, six two-way ANOVA interaction tests of log-transformed Mg^{2+} IC_{50} data were performed (one test per voltage; **Fig. 8**). Although untransformed IC_{50} measurement data do not follow a normal distribution, log-transformed IC_{50} data are normally distributed[49]. Because ANOVA tests assume normal distributions of data, the log transformation was used. The factors in each two-way ANOVA were GluN1 subunit identity (wild type or mutant) and GluN2A subunit identity (wild type or mutant). A significant interaction effect implies that the magnitude of the effect of one factor (for example, mutation of GluN1 subunit) depended on the other factor (for example, the identity of the coexpressed GluN2A subunit), which would reflect coupling between the mutated GluN1 and GluN2A residues. Interactions were considered to be significant at $P < 0.05$ (significance level $\alpha = 0.05$).

The percent of the difference between GluN1/2A and GluN1/2D receptor Mg^{2+} IC_{50} that was accounted for by mutation of the GluN2 S/L site was calculated for the GluN2A(S632L) mutation (88%; see Results) using the equation

$$(3)\quad 100\times\frac{\log(Mg^{2+}IC_{50}\,\text{GluN1/2A(S632L)})-\log(Mg^{2+}IC_{50}\,\text{GluN1/2A})}{\log(Mg^{2+}IC_{50}\,\text{GluN1/2D})-\log(Mg^{2+}IC_{50}\,\text{GluN1/2A})}$$

A related equation was used to calculate the percent of the difference between Mg^{2+} IC_{50} of GluN1/2A and of GluN1/2C or GluN1/2D receptor accounted for by the GluN2C(L643S) mutation (67%) and the GluN2D(L657S) mutation (57%). Although using log-transformed IC_{50} data is the more appropriate approach[50], we performed similar calculations without log transformation, yielding 81% for the GluN2A(S632L) mutation, 73% for the GluN2D(L657S) mutation and 77% for the GluN2C(L643S) mutation.

44. Clarke, R.J. & Johnson, J. NMDA receptor NR2 subunit dependence of the slow component of magnesium unblock. *J. Neurosci.* **26**, 5825–5834 (2006).
45. Colquhoun, D. & Sigworth, F.J. Analysis of single ion channel data. in *Single-Channel Recording* (eds. B. Sakmann & E. Neher) 483–587 (Plenum Press, New York, 1995).
46. Humphrey, W., Dalke, A. & Schulten, K. VMD: visual molecular dynamics. *J. Mol. Graph.* **14**, 33–38 (1996).
47. R Development Core Team. *R: A Language and Environment for Statistical Computing* (R Foundation for Statistical Computing, Vienna, 2011).
48. Heiberger, R.M. & Holland, B. *Statistical Analysis and Data Display: An Intermediate Course with Examples in S-plus, R, and SAS* (Springer, New York, 2004).
49. Fleming, W.W., Westfall, D.P., De la Lande, I.S. & Jellett, L.B. Log-normal distribution of equieffective doses of norepinephrine and acetylcholine in several tissues. *J. Pharmacol. Exp. Ther.* **181**, 339–345 (1972).
50. Colquhoun, D. Binding, gating, affinity and efficacy: the interpretation of structure-activity relationships for agonists and of the effects of mutating receptors. *Br. J. Pharmacol.* **125**, 924–947 (1998).

© 2012 Nature America, Inc. All rights reserved.